MEASURING THE DISTANCE BETWEEN EPIDEMIC GROWTH MODELS

RAIMUND BÜRGER[A], GERARDO CHOWELL[B,C,D], AND LEIDY YISSEDT LARA-DÍAZ[A,*]

Abstract. Phenomenological growth models provide a framework for characterizing epidemic trajectories, estimating key transmission parameters, gaining insight into the contribution of various transmission pathways, and providing long-term and short-term forecasts. Such models only require a small number of parameters to describe epidemic growth patterns. They can be expressed by an ordinary differential equation (ODE) of the type $C'(t) = f(t;\Theta)$ for $t > 0$, $C(0) = C_0$, where t is time, $C(t)$ is the total size of the epidemic (the cumulative number of cases) at time t, C_0 is the initial number of cases, f is a model-specific incidence function, and Θ is a vector of parameters. The current COVID-19 pandemic is a scenario for which such models are of obvious importance. In [R. Bürger, G. Chowell, L.Y. Lara-Díaz, Math. Biosci. Eng. 16 (2019) 4250–4273] it is demonstrated that some models are better at fitting data of specific epidemic outbreaks than others even when the models have the same number of parameters. This situation motivates the need to quantify the distance between two models as a measure of differences in the dynamics that each model is capable of generating. The present work contributes to a systematic study of differences between models and how such differences may explain the ability of certain models to provide a better fit to data than others. To this end metrics are defined that describe the differences in the dynamics between different dynamic models. These metrics are based on a concept of distance of one growth model from another one that quantifies how well the former fits data generated by the latter. This concept of distance is, however, not symmetric. The procedure of calculating distances is applied to synthetic data and real data from influenza, Ebola, and COVID-19 outbreaks.

1. Introduction

1.1. **Scope.** A wide variety of mathematical models have been used to study the patterns of growth processes of populations and epidemics in humans, animals, and plants [1–14]. Here we are especially interested in dynamic growth models that provide a framework for characterizing epidemic trajectories, estimating key transmission parameters, gaining insight into the contribution of various transmission pathways, and providing long-term and short-term forecasts. The recent monograph by Yan and Chowell [15] provides an introduction to the topic. We herein focus on phenomenological models that only require a small number of parameters are commonly used to describe epidemic growth patterns, and which can be expressed by an ordinary differential equation (ODE) of the

Date: May 23, 2020.

Key words and phrases. Epidemic growth model, logistic model, Richards model, Gompertz model, distance, simulated annealing.

*Corresponding author.

[A]CI^{2}MA and Departamento de Ingeniería Matemática, Facultad de Ciencias Físicas y Matemáticas, Universidad de Concepción, Casilla 160-C, Concepción, Chile. E-Mail: rburger@ing-mat.udec.cl, llara@ing-mat.udec.cl.

[B]School of Public Health, Georgia State University, Atlanta, Georgia, USA.

[C]Simon A. Levin Mathematical and Computational Modeling Sciences Center, School of Human Evolution and Social Change, Arizona State University, Tempe, AZ 85287, USA.

[D]Division of International Epidemiology and Population Studies, Fogarty International Center, National Institutes of Health, Bethesda, MD 20892, USA.

type

$$C'(t) := \frac{\mathrm{d}C(t)}{\mathrm{d}t} = f(t;\Theta), \quad t > 0; \quad C(0) = C_0, \tag{1.1}$$

where t is time, $C(t)$ is the total size of the epidemic (the cumulative number of cases) at time t, C_0 is the initial number of cases, f is an incidence function that is specific to each growth model under study, and Θ is a vector of parameters. Such models have been used to study the epidemics of influenza [16–18], Ebola [19–21], Zika [22,23], and others of global interest. The current COVID-19 pandemic is a scenario for which such models are of obvious importance [24–27].

In [16] we demonstrate that some models are better at fitting data of specific epidemic outbreaks than others even when the models have the same number of parameters. Consider, for instance, the three-parameter so-called generalized logistic model (GLM) specified by

$$f(t;\Theta) = rC(t)^p\big(1 - C(t)/K\big), \quad \Theta = (r, p, K), \tag{1.2}$$

where the parameter $r > 0$ indicates the growth rate (its dimension is 1/time), K is the size of the epidemic, and $p \in [0, 1]$ is a growth scaling parameter that indicates the kind of growth (e.g., exponential vs. sub-exponential). In the comparative analysis between two models and their generalizations [16], the GLM was able to capture the trajectories for 37 real datasets describing the progression of epidemic outbreaks. In fact, this model showed to have the smallest error between the data and the fit, and the estimated parameters were identifiable, that is, the average value of each parameter was effectively a central value in the confidence intervals, where we used the definitions and calculations introduced in [28] for the error and the confidence intervals.

Although several growth models could be considered for a given dataset, little work has been conducted to analyze the differences between models. Here we define the distance between two models as a measure of differences in the dynamics that each model is capable of generating. We address questions such as whether the dynamics of the logistic growth model (LM), defined by

$$f(t;\Theta) = rC(t)\big(1 - C(t)/K\big), \quad \Theta = (r, K), \tag{1.3}$$

is more similar to that of the Gompertz model (GoM), corresponding to

$$f(t;\Theta) = rC(t)\exp(-bt), \quad \Theta = (r, b), \tag{1.4}$$

where the parameter $b > 0$ describes the exponential decay of the growth rate r, or to that of the Richards model (RM)

$$f(t;\Theta) = rC(t)\big(1 - (C(t)/K)^p\big), \quad \Theta = (r, K, p). \tag{1.5}$$

There is a need to develop metrics that help quantify the differences in the dynamics obtained from different models that aim to capture growth processes in the social and natural sciences. Such metrics can be helpful to assess which models are more parsimonious than others in different contexts. In the context of epidemic modeling, many models have been developed to investigate the transmission dynamics and control of infectious diseases [10,14,29]. However, there has not been a systematic study of differences between models and how differences in dynamics may explain the ability of certain models to provide a better fit to data than others. Here we aim to make progress in this direction by focusing on simple models that strive to capture many of the empirical patterns found in epidemic data.

To address these questions we define metrics of the differences in the dynamics between different dynamics models of the form (1.1). Here we employ simulated data for three generalized growth models (namely GLM, GGoM and RM), and with the help of mathematical and computational methods we calculated the fit and performance metrics in terms of which the distances are defined.

As we will show, it turns out that the GLM is closer to the dynamics of the RM. On the other hand, the generalized Gompertz model (GGoM) defined by

$$f(t;\Theta) = rC(t)^p \exp(-bt), \quad \Theta = (r, b, p). \tag{1.6}$$

is the farthest from the RM and GLM. This is because the scaling parameter (p in (1.2), (1.5) and (1.6)) plays a more significant role in the GLM since its variation within the GLM causes more changes in its dynamics than for the other growth models.

The concept of measuring the distance between two models, say A and B, is based on simulation study that we introduce in the following sections.

1.2. **Related work.** To illustrate how models can support different features of epidemic data, we can refer to the scaling of epidemic growth that characterizes the early growth dynamics of epidemics. While some epidemics spread rapidly through a population following an exponential growth phase such as pandemic influenza or the ongoing epidemic of the novel coronavirus emerging from China (COVID-19) [24], some outbreaks spread more slowly as a result of the mode of transmission or the contact network through which the pathogen spreads. For instance, sexually transmitted diseases and Ebola do not spread through the air, but require a specific type of intimate contact to spread. In such situations the disease is expected to spread follow sub-exponential growth patterns. When a model only supports exponential growth dynamics, we could expect differences between such a model and more flexible models that can capture a range of early epidemic growth dynamics [30].

One important step in our treatment consists in generating a fit of one of the growth models to data that are either generated by another growth model or using real outbreak data. Since the parametric forms of growth models are essentially non-linear, standard least-squares methods are often not applicable. Thus, to provide these fits, we resort to the Simulated Annealing (SA) method. This method is defined in [31] as a powerful stochastic search method applicable to a wide range of problems that occur in a variety of disciplines including physics, engineering problems, mathematical programming, and statics. The problem can be formulated as follows. Suppose we are given finite-dimensional solution space $\mathcal{S}$, and a function $f : \mathcal{S} \to \mathbb{R}$, and we want find an optimal configuration $x^* \in \mathcal{S}$ such that $f(x^*) = \min_{x\in\mathcal{S}} f(x)$. This method has become very popular because the algorithm can solve unconstrained and bound-constrained optimization problems, especially in the multidimensional case when the objective function may have many local extremes and may not be smooth. In that case, SA is advantageous because it does not require calculation of derivatives, and thus be considered as a derivative-free method. In papers including [32, 33] this method has been used to parameter estimation, which motivated our computation.

1.3. **Outline of the paper.** In the next sections we define the growth models considered in our study as well as the numerical method for parameter estimation and the quantification of the distance between two models. The concept of distance from one growth model to another is detailed in Section 2. To this end we summarize in Section 2.1 properties of the models under consideration and recall explicit solutions wherever available. Then, in Section 2.2 we outline the procedure to measure the distance from a phenomenological growth model B to another phenomenological growth model A, denoted by $\mathrm{dist}(B \to A)$, which we summarize in Algorithm 2.1. A crucial role within this algorithm is played by the SA method (utilized to find the optimal parameters for model B when fitting a dataset generated by model A), which is briefly discussed in Section 2.3. Next, in Section 3 we apply the methodology to four growth models: LM, GLM, RM (with logistic growth) and GGoM introduced in Section 1.1 considering synthetic datasets (as outlined in Section 2.2). Specifically, we introduce in Section 3.1 the parameters and solution spaces for each of these models,

Growth model	Parameters
Logistic growth model (LM)	$\Theta = (\theta_1 = r, \theta_2 = K);\ r, K > 0$
Generalized Logistic growth model (GLM)	$\Theta = (\theta_1 = r, \theta_2 = K, \theta_3 = p);\ r, K > 0,\ p \in [0, 1]$
Richards model (RM)	$\Theta = (\theta_1 = r, \theta_2 = K, \theta_3 = p);\ r, K > 0,\ p \in [0, 1]$
Generalized Gompertz model (GGoM)	$\Theta = \{\theta_1 = r, \theta_2 = b, \theta_3 = p\};\ r, b > 0,\ p \in [0, 1]$

TABLE 1. Summary of information on models and parameters.

with special emphasis on the exponent p. The specific application of the SA method is discussed in Section 3.2. Then, in Sections 3.3 to 3.6 we present Experiments 1, 2, 3, and 4 in which we calculate distances from the LM, RM, GLM, and GGoM to other models, respectively. In Section 4 we apply the methodology to real data of outbreaks of influenza, Ebola, and COVID-19. Some conclusions are collected in Section 5.

2. Distance between growth models

2.1. **On growth models.** For the growth models summarized in Table 1, $p = 0$ corresponds to a constant incidence over time, $p = 1$ corresponds to exponential growth, and any intermediate value $0 < p < 1$ leads to a model that describes initial sub-exponential growth dynamics [30, 34–36]. Three of these models have an initial logistic growth because when $p = 1$ for the GLM and RM, in other words the LM is recovered, in contrast, this is not the case for the GGoM. (The RM and GLM show two forms of incorporating the parameter p to the LM model to obtain the generalized growth form $rC^p(t)$.) With all these models our interest is to measure how close the logistic models are to each other and to the GGoM, and to assess whether two or three parameters are sufficient to recover other dynamics. We recall that these models have the following explicit solutions. The solution of the LM (1.1), (1.3) is given by

$$C(t) = \frac{KC(0)\exp(rt)}{K + C(0)(\exp(rt) - 1)}, \tag{2.1}$$

that of the GoM (1.1), (1.4) (that is, the GGoM for $p = 1$) by

$$C(t) = C(0)\exp\big((r/b)\big(1 - \exp(-bt)\big)\big), \tag{2.2}$$

while for the GGoM (1.1), (1.4) we get

$$C(t) = \big((1-p)(r/b)\big(1 - \exp(-bt)\big) + C(0)^{1-p}\big)^{1/(1-p)} \quad (\text{where } 0 < p < 1). \tag{2.3}$$

The solution of the RM (1.1), (1.5) is

$$C(t) = \frac{KC(0)\exp(rt)}{(K^p + C(0)^p(\exp(prt) - 1))^{1/p}}. \tag{2.4}$$

As is pointed out in [16], the GLM (1.1), (1.2) does not have a solution in closed algebraic form for general values $p \in (0, 1)$. (This point is also discussed in detail in [37]; the Pütter-Bertalanffy growth equation studied in that paper includes (1.1), (1.2) as a special case.) For the GLM we solve the initial-value problem (1.1) numerically whenever necessary.

Phenomenological growth models can capture epidemic growth patterns, through the relationship between the case incidence curve and the cumulative incidence curve. The integrated version of

(1.1), namely

$$C(t) = C(0) + \int_0^t f(\tau;\Theta)\,\mathrm{d}\tau, \quad t > 0,$$

can be approximated by the following formula if we assume that values of the incidence function $f(t;\Theta)$ are given at discrete times $t = t_k$, $k = 1,\dots,n$ only:

$$C(t_k) \approx C(0) + \sum_{l=1}^{k}(t_l - t_{l-1})f(t_l;\Theta), \quad k = 1,2,\dots,n, \quad t_0 = 0,$$

with $t_k \in [0,T]$. Thus, we may recover the cumulative curve $t \mapsto C(t)$ in terms of tabulated values of the incidence function $f(t;\Theta)$, and similarly we may approximate $f(t_k;\Theta)$ in terms of given discrete values $C(t_k)$ as follows:

$$f(t_k;\Theta) \approx \frac{C(t_k) - C(t_{k-1})}{t_k - t_{k-1}}, \qquad k = 1,2,\dots,n, \qquad \text{with} \qquad f(t_0;\Theta) = C(t_0). \tag{2.5}$$

2.2. **Measuring the distance between growth models.** To determine $\mathrm{dist}(B \to A)$, we start by defining S parameter sets Θ_j, $j = 1,\dots,S$ for model A for which we determine the incidence curves, that is, we compute the (exact or numerical) solutions for the ODE (1.1) for model A for each parameter set Θ_j, and these are our datasets to fit model B. We fit model B to each of these curves by using the matlab function SIMULANNEALBND for Q different initial parameter sets of model B. These initial parameter sets, in turn, are created by using the matlab function LHSDESIGN that creates Q random values within a defined range. For instance, for the parameter K we create $Q = 10$ values between 0 and 1000. Assume now that y_{t_i}, $i = 1,\dots,n$, are the points or data for each time t_i of model A, and $f(t_i,\hat{\Theta})$, are the values of fits obtained with model B, where $\hat{\Theta}$ is the set of estimated parameters of model B. Then we determine the root mean square error (RMSE)

$$\mathrm{RMSE} := \sqrt{\frac{1}{n}\sum_{i=1}^{n}\big(f(t_i,\hat{\Theta}) - y_{t_i}\big)^2}$$

to compute the distance between the data curve, tabulated at $t_1,\dots,t_n$, and a fit with model B expressed by the values $f(t_i,\hat{\Theta})$, $i = 1,\dots,n$. We select the best fit with the smallest RMSE between the Q fits for each of the S data curves (see Figure 1), and then consider the mean of the S best values of RSME as the distance from model B to model A. Besides, we will also calculate the sum of squared errors (SSE) given by

$$\mathrm{SSE} = \sum_{i=1}^{n}\big(f(t_i,\hat{\Theta}) - y_{t_i}\big)^2,$$

because this metric naturally arises in the context of least-squares methods. The necessary computations are summarized in Algorithm 2.1 and in Figure 2.

Algorithm 2.1 (Calculating $\mathrm{dist}(B \to A)$)**.**

Input:

- *Parameter sets* $\{\Theta_j\}_{j=1,\dots,S}$ *of model A that define the incidence curves* $\{f_A(t;\Theta_j)\}_{j=1,\dots,S}$, $t \in [0,T]$ *(simulated data).*
- *Initial parameter sets* $\{\Theta_{B,i}\}_{i=1,\dots,Q}$ *of model B.*
- *Sampling times* t_k, $k = 1,\dots,n$ *at which the incidence curves (both of the simulated data and the approximation) are evaluated.*

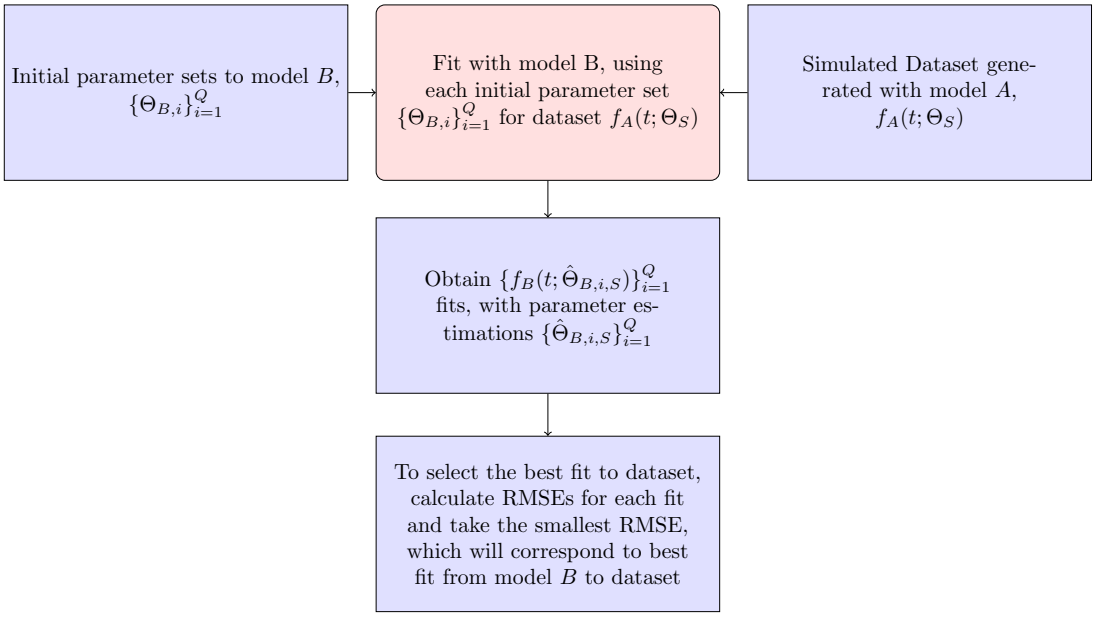

FIGURE 1. Process to fit the model B to dataset $f_A(t;\Theta_S)$ generated with model A.

for $j = 1, \ldots, S$
  $i^*(j) \leftarrow 1$
  for $i = 1, \ldots, Q$
    (1) *Determine the vector of estimated parameters* $\hat{\Theta}_{B,i,j}$ *for the* j*-th data curve based on the initial parameter vector* $\Theta_{B,i}$ *by Simulated Annealing.*
    (2) *Calculate*

$$\mathrm{RMSE}_{ij} = \sqrt{\frac{1}{n}\sum_{k=1}^{n}\big(f_B(t_k;\hat{\Theta}_{B,i,j}) - f_A(t_k;\Theta_j)\big)^2}.$$

    (3) **if** $\mathrm{RMSE}_{ij} \leq \mathrm{RMSE}_{i^*(j),j}$ **then**
      $i^*(j) \leftarrow i$
    endif
  endfor
endfor
Output: the distance from model B *to model* A*,*

$$\mathrm{dist}(B \to A) \leftarrow \frac{1}{S}\sum_{j=1}^{S}\mathrm{RSME}_{i^*(j),j}.$$

2.3. **Simulated Annealing method for parameter estimation.** As we want know the distance between two growth models, we need numerical methods to calculate the fits from a model B to a model A and in some cases to determine solutions of the ODEs. Then to achieve the best fit it is necessary to estimate parameters, for which we employ the SA method to minimize the Euclidean distance between the curve from model A and the fit with the estimation parameters of model B.

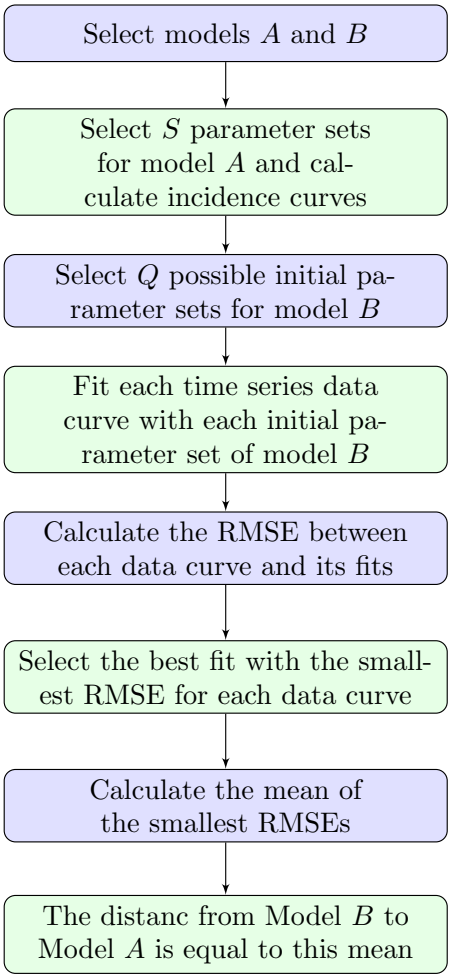

FIGURE 2. Step by step for measure the distance between two models.

This method is used through the matlab function SIMULANNEALBND for parameter estimation, where the goal is to minimize the function

$$\Theta \mapsto J(\Theta) := \sqrt{\sum_{k=1}^{n} \big(f(t_k;\Theta) - \mathrm{data}_{t_k}\big)^2},$$

where $t \mapsto f(t;\Theta)$ is the incidence function of a growth model evaluated for a parameter vector Θ that should satisfy $\Theta \in \mathcal{S}$ for some admissible set $\mathcal{S}$ compatible with the algebraic form of f for n different time points t_k, where data_{t_k} correspond to data in time series. In our case, the values $\{\mathrm{data}_{t_k}\}_{k=1,\dots,n}$ are the datasets generated by model A, and model B will define the incidence function f and the set $\mathcal{S}$. Hence, the optimization problem at hand can be defined as follows:

$$\text{find } \hat{\Theta} \in \mathcal{S} \text{ such that } J(\hat{\Theta}) = \min_{\Theta \in \mathcal{S}} J(\Theta). \tag{2.6}$$

3. Application of the methodology

3.1. **Parameters of specific growth models.** The methodology of Section 2.2 will allow us to determine the contribution of the scaling parameter p and to observe the closeness between the dynamics of the models A and B, where model $A \in \{\mathrm{GLM}, \mathrm{RM}, \mathrm{GGoM}\}$ is used to generate simulated data or data curves and model $B \in \{\mathrm{LM}, \mathrm{GLM}, \mathrm{RM}, \mathrm{GGoM}\}$, $B \neq A$, is employed to calculate fits. To assess the contribution of the parameter p, we select a set of values of p fairly close to 1 but leave other parameters fixed (taking into account that the parameter b of the GGoM depends on the value of p). Then, we analyze the distance of model B to curves generated with model A. For example, if we consider $B = \mathrm{LM}$ and its fits to each data curve generated with model A, we can calculate the RMSEs and finally to have the distance from LM model to GLM, RM and GGoM curves.

Furthermore, we also calculate the distance from GLM model to RM and GGoM curves, RM model to GLM and GGoM curves and finally from GGoM model to GLM and RM curves. These processes will be named Experiment 1, 2, 3, and 4, respectively.

For the experiments we consider the three parameters r, p, and K. To compare models with equivalent parameters, we choose (as in [16, Sect. 1]) the following expressions for the parameters b and r within the GGoM in terms of the parameter K and the initial value $C(0)$:

$$r = 1 - \frac{C(0)}{K}, \tag{3.1}$$

$$b = \begin{cases} \dfrac{r}{\log(K/C(0))} & \text{if } p = 1, \\ \dfrac{r(1-p)}{K^{1-p} - C(0)^{1-p}} & \text{if } 0 < p < 1, \end{cases} \tag{3.2}$$

where the expression for $p = 1$ is the limit of that for $0 < p < 1$, i.e.,

$$\frac{r}{\log(K/C(0))} = \lim_{p \to 1, p<1} \frac{r(1-p)}{K^{1-p} - C(0)^{1-p}}.$$

Therefore, to standardize the analysis, we consider the parameter set $\Theta = (r, p, K)$ for all models with $K = 1000$, $C(0) = 1$, r determined by (3.1), and b calculated from (3.2) in dependence of the value of the parameter p, which is allowed to assume one of the values

$$p \in \mathcal{P} := \{1, 0.995, 0.99, 0.98, 0.95, 0.85, 0.8\}.$$

Summarizing, we utilize the parameters

$$(r, p, K) = (0.999, p, 1000) \quad \text{with } p \in \mathcal{P}.$$

These values are used directly for the GLM and RM, while for the GGoM we employ the corresponding parameters $(r, p, b) = (0.999, p, b)$ with $b = 0.1446$ if $p = 1$ and $b = 0.1421$, 0.1397, 0.1349, 0.1211, 0.0824, and 0.0670 for $p = 0.995$, 0.99, 0.98, 0.95, 0.85, and 0.8, respectively.

These parameters, listed also in Table 2, produce the data curves shown in Figure 3. Roughly speaking, these curves illustrate that the role of the parameter p within the GGoM and GLM is to describe the initial growth of the incidence curve, while within the RM the initial phase of the curves, where values of $C(t)$ are still fairly small, is almost the same for all p-values. Furthermore, we see that with decreasing values of p the extremal value (peak) of the incidence curves of the GGoM and GLM decreases rapidly, while that of the RM model decreases only slowly. In addition, the GGoM and GLM exhibit an appreciable shift of the timing of that maximum (i.e., the peak time increases significantly with decreasing p) while this effect is not much appreciable for the RM (with the chosen parameters). (For the GGoM and RM the respective closed formulas for $C(t)$,

Parameters for GGoM curves			Parameters for RM curves			Parameters for GLM curves		
r	b	p	r	p	K	r	p	K
0.999	0.1446	1.000	0.999	1.000	1000	0.999	1.000	1000
0.999	0.1421	0.995	0.999	0.995	1000	0.999	0.995	1000
0.999	0.1397	0.990	0.999	0.990	1000	0.999	0.990	1000
0.999	0.1349	0.980	0.999	0.980	1000	0.999	0.980	1000
0.999	0.1211	0.950	0.999	0.950	1000	0.999	0.950	1000
0.999	0.0824	0.850	0.999	0.850	1000	0.999	0.850	1000
0.999	0.0670	0.800	0.999	0.800	1000	0.999	0.800	1000

TABLE 2. Summary of parameters for each model curves

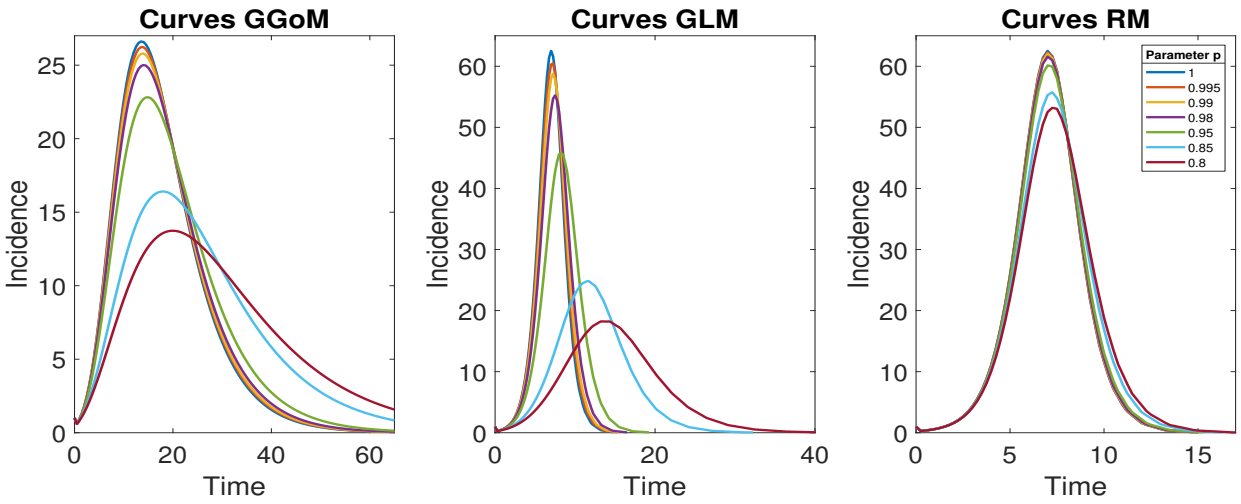

FIGURE 3. Data curves for each growth model.

Model B			
LM $\Theta = (r, K)$	GLM $\Theta = (r, p, K)$	RM $\Theta = (r, p, K)$	GGoM $\Theta = (r, b, p)$
$(0, 4) \times (0, 1000]$	$(0, 4) \times (0, 1] \times (0, 1000]$	$(0, 4) \times (0, 1] \times (0, 1000]$	$(0, 4) \times (0, 1] \times (0, 1]$

TABLE 3. Initial parameter set for each model B

(2.3) and (2.4), may be utilized and differentiated to discuss all these properties in explicit form, see [16].)

To help the fits, we generate the data curves from model A, with evaluations for every $0 < h < 1$ time units to have more points or data for fit model B in each case, i.e. we select $t_k = kh$, $k = 0, 1, 2, 3, \ldots, n$. For example, we use temporal meshwidth of $h = 0.25$ for the GLM curves.

3.2. **Application of the Simulated Annealing (SA) method.** The SA method will be used to estimate parameters via the Matlab function SIMULANNEALBND. The objective function to minimize is (2.6) for parameter vectors Θ and functions f that depend on the choice of model B in

Model B \ Model A	GLM curves	RM curves	GGoM curves
LM (r, K)	$[0.5, 1.1] \times (700, 1010)$	$[0.9, 1.1] \times (900, 1010)$	$[0.2, 0.5] \times [400, 800]$
GLM (r, p, K)		$[0.8, 1] \times [0.2, 1] \times [500, 1010)$, $0.99 \leq p \leq 1$; $[0.5, 1.5] \times [0.4, 0.85] \times [800, 1010)$, $0.95 \leq p < 0.99$; $[0.5, 1] \times [0.4, 0.999] \times [900, 1010)$, $0.8 \leq p < 0.95$	$[1.5, 1.6] \times [0.5, 0.7] \times [800, 1000]$
RM (r, p, K)	$[0.7, 0.99] \times [0.2, 0.999] \times [800, 1010)$		$[1.8, 1.9] \times [0.05, 0.08] \times [800, 1000]$, $0.95 \leq p \leq 1$ $[1.8, 2] \times [0.05, 0.08] \times [800, 1010)$, $0.8 \leq p \leq 0.25$
GGoM (r, b, p)	$(0, 3) \times (0, 1] \times (0, 1]$	$(0, 3) \times (0, 1] \times (0, 1]$	

TABLE 4. Solution spaces for the parameter estimation with each model B and data curves.

each case. For simplicity, the application of SIMULANNEALBND we will use the solutions from model B, where by utilizing the equation (2.5), we could recover f in terms of C.

For example, the function f within the objective function for $B =$ LM is calculated used the solution C to LM model presented in (2.1), i.e. we use the explicit solution of this model, as we also do for the RM with (formula (2.4)) and GGoM with (formulas (2.2) and (2.3) for the respective cases $p = 1$ and $0 < p < 1$). However, since the GLM does not have a solution in closed algebraic form we employ the matlab ODE23S procedure to solve the initial value problem to the GLM.

Then, once the form of the algebraic model under study is given, we need to define the solution spaces for each model which depend on the role of each parameter within each model function. Here the quantities K, $C(0)$, and p are fixed and the expressions for the parameters r and b are given by (3.1) and (3.2), respectively. To search the solution spaces for each parameter, we consider the conditions summarized in Table 1 to define the sets specified in Table 3, where we select the initial parameter to run the SA algorithm. This algorithm provides a solution that varies from run to run since the algorithm consists in a random process that utilizes a probability criterion to select the optimal value. However, if we apply the SA algorithm to Q possible initial parameter sets, then with these solutions we can reduce or limit the solution space between the maximum and the minimum best parameters shown for the run. This new solution space helps us to control results and improve the solution and the calculation time. This process follows the idea shown in [32] concerning double cycle application of SA. The solution spaces that result from the fits for each model B with each data curve are summarized in Table 4.

3.3. **Experiment 1: distances from the logistic model (LM) to other models.** With the best set of initial parameters and the best parameter estimation, we have Figure 4 with the best fits for the LM, where we can see that the LM is closer to the RM curves, since it captures this dynamics better than for that of the other models. On the other hand, LM is further from GGoM curves, this is due to the long time defined for GGoM data, that the LM exceeds the maximum given by it. Similar situation occur when maximum decrease for GLM curves and the time increase. The RMSEs calculated to measure the distance are shown in Table 5 and Figure 5. It turns out that that when the value of p is decreased for the GLM and RM, the error increases more for the GLM than for the RM while a different situation occurs with the GGoM, since the error decreases when p is decreased, but this change is slower than the increase of the error for the GLM and RM. The increase of the RMSE for data generated by the LM is expected because when $p = 1$, the

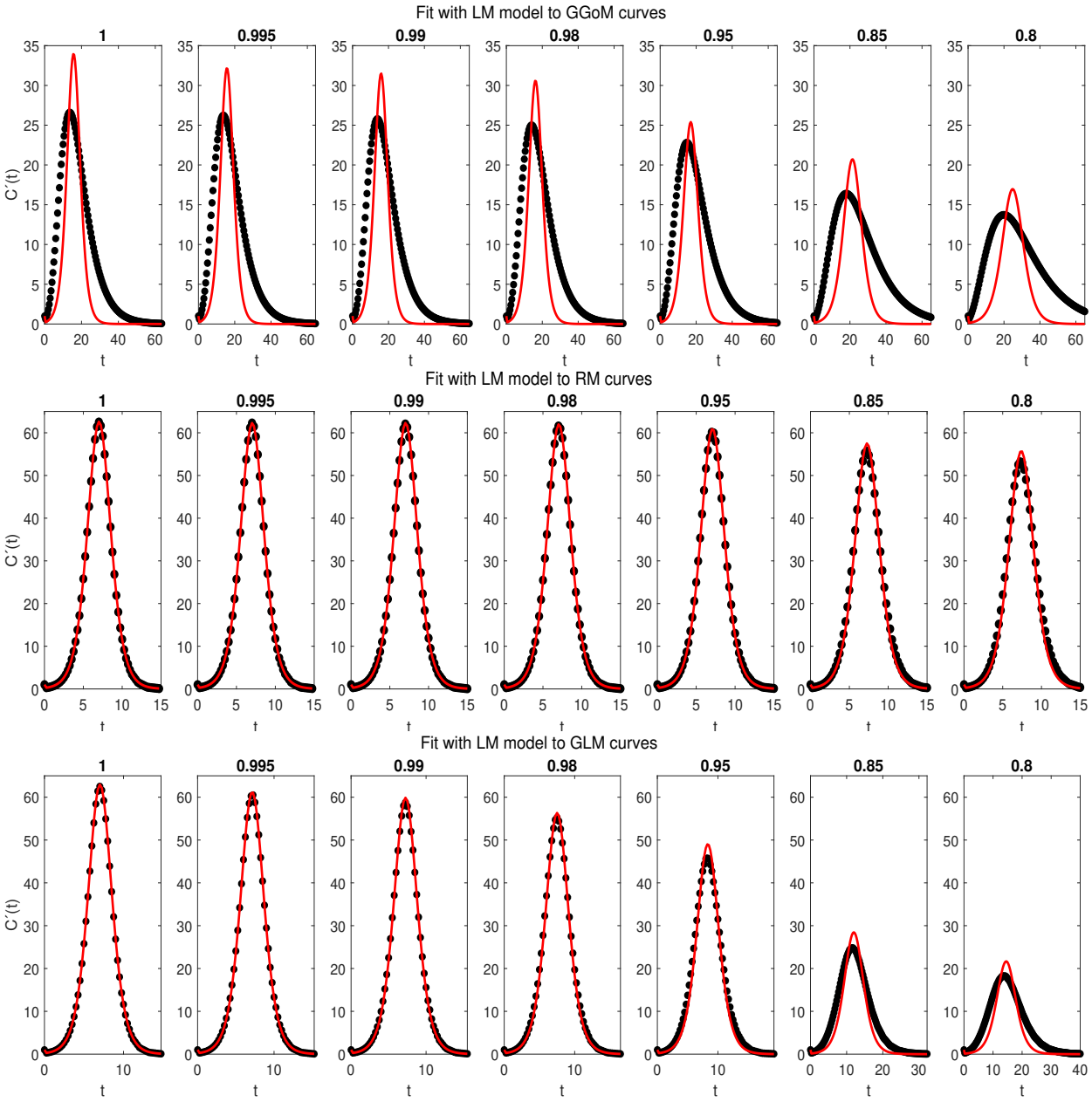

FIGURE 4. Experiment 1: results of fits of the LM (model B) to the curves of data generated by the GGoM (top row), GLM (middle row), and GLM (bottom row), for the indicated values of p.

dynamics of the LM and that of these models should be the same, where in Table 6 (first row) we can see that the parameter estimation for GLM and RM data curves with $p = 1$ are closer to real parameters, i.e., to $\Theta = (r = 0.999, p = 1, K = 1000)$. Another observation about results for parameter estimation summarized in Table 6 is that the growth rate r of the LM for data curves generated by the GGoM is naturally smaller than the growth rate for data generated by the LM,

Model B	Model A	Error RMSE to each fit with model B $p=1$	$p=0.995$	$p=0.99$	$p=0.98$	$p=0.95$	$p=0.85$	$p=0.8$	dist$(B \to A)$
LM	GGoM	5.2319	5.1864	5.1430	5.1163	5.0480	4.7069	4.4697	5.1163
	GLM	0.1900	0.2455	0.4625	0.8184	1.7021	2.6900	2.6570	0.8184
	RM	0.0568	0.0685	0.0955	0.1706	0.4099	1.1989	1.5615	0.1706
RM	GGoM	0.6827	0.6804	0.7055	0.7668	0.9285	1.3375	1.4244	0.7668
	GLM	0.0037	0.0381	0.0741	0.1347	0.2638	0.3397	0.3066	0.1347
GLM	GGoM	0.4712	0.4757	0.4556	0.4481	0.4284	0.3513	0.3015	0.4481
	RM	0.0069	0.1536	0.0605	0.1993	0.2477	0.7268	1.6235	0.1993
GGoM	GLM	12.1578	11.6221	11.1988	10.2038	7.8028	3.4788	1.8623	10.2038
	RM	12.1667	12.1529	12.0017	12.0359	11.4630	10.1060	9.3656	12.0017

TABLE 5. RSME for each data curve, where columns 3 to 9 correspond to the error for the indicated value of p, and column 10 shows the mean RMSE, that is, dist$(B \to A)$.

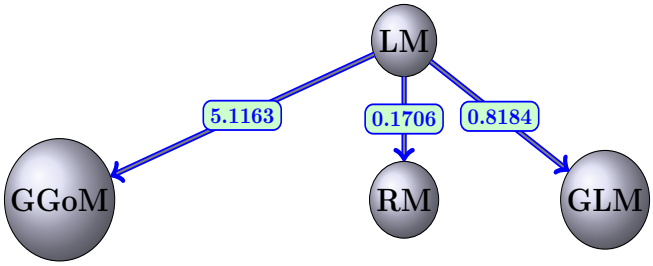

FIGURE 5. Experiment 1: illustrative diagram for the distances dist(LM $\to$ GGoM), dist(LM $\to$ RM), and dist(LM $\to$ GLM) based on data curves.

Parameter Estimation for LM						
CURVES	with GGoM curves		with GLM curves		with RM curves	
with p	r	K	r	K	r	K
1	0.4193	621.2245	1.0017	1007.1734	1.0012	1001.6787
0.995	0.4149	617.9446	0.9836	997.3534	0.9999	998.2173
0.99	0.4105	617.1784	0.9662	992.6324	0.9989	999.1522
0.98	0.4018	610.0832	0.9310	969.1496	0.9965	996.8109
0.95	0.3756	598.7651	0.8341	941.6386	0.9888	987.6975
0.85	0.2931	554.6741	0.5643	806.5594	0.9600	959.6222
0.8	0.2550	535.9005	0.4597	754.1879	0.9433	946.7694

TABLE 6. Experiment 1: parameter estimation for LM with GGoM, GLM and RM data curves.

because the GGoM has a slower increase, where for the same reason for GLM data with $p = 0.8$ the growth rate decreases to 0.4597.

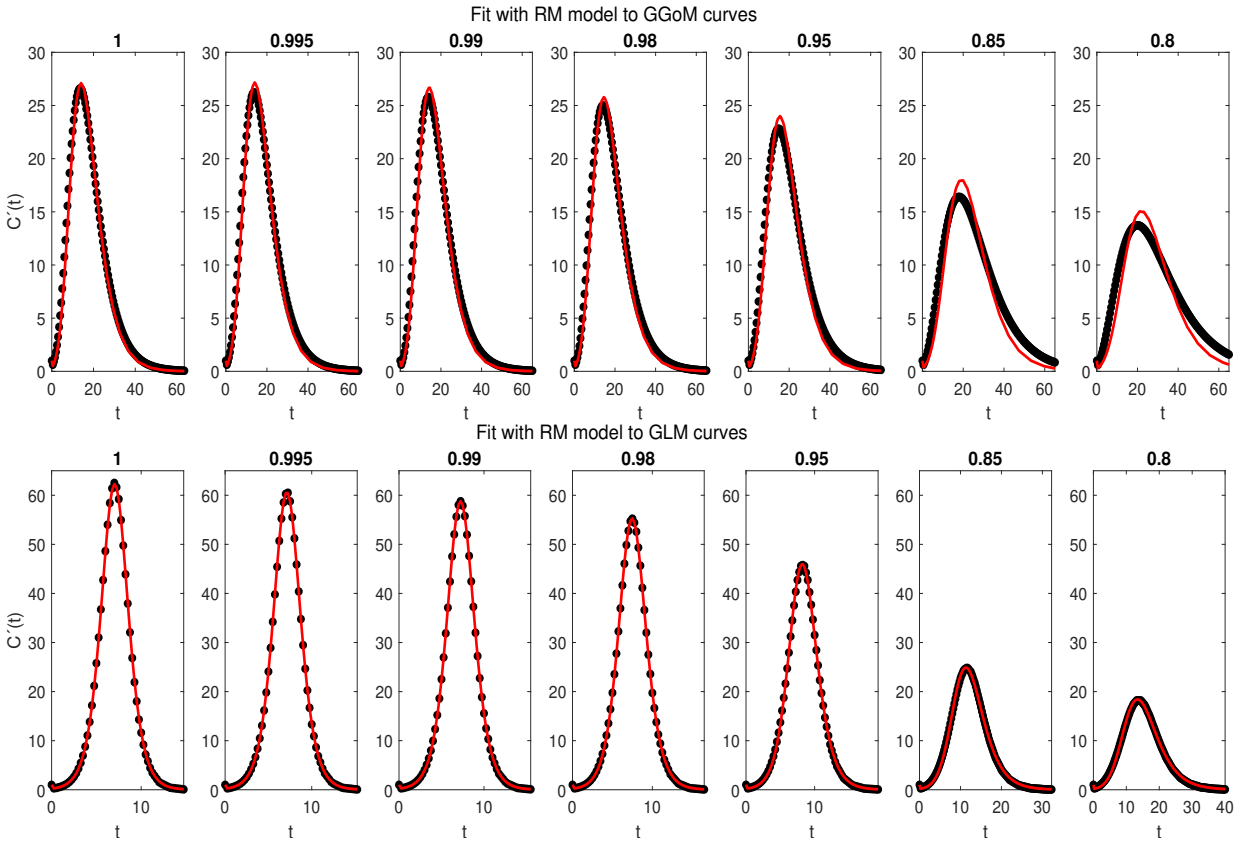

FIGURE 6. Experiment 2: results of fits of the RM (model B) to the curves of data generated by the GGoM (top row) and the GLM (bottom row), for the indicated values of p.

Parameter Estimation for RM						
CURVES	with GGoM curves			with GLM curves		
with p	r	p	K	r	p	K
1	1.9998	0.0800	954.1139	0.9990	0.9999	1000.0513
0.995	1.9999	0.0798	957.9978	0.9876	0.9732	999.5539
0.99	1.9973	0.0789	953.8977	0.9763	0.9476	999.4866
0.98	1.9912	0.0771	944.5345	0.9547	0.8976	997.8995
0.95	1.9431	0.0740	937.1508	0.9000	0.7532	1000.3445
0.85	1.8952	0.0593	892.6791	0.8000	0.4048	998.1613
0.8	1.9238	0.0500	869.3741	0.8551	0.2612	1003.6135

TABLE 7. Experiment 2: parameter estimation for RM with GGoM and GLM data curves.

3.4. **Experiment 2: distances from the Richards model (RM) to other models.** We follow the structure of presentation of results of Experiment 1. In Figure 6 we can observe that the RM (in the role of model B) is closer to the GLM than to the GGoM, where the fits captures almost all the

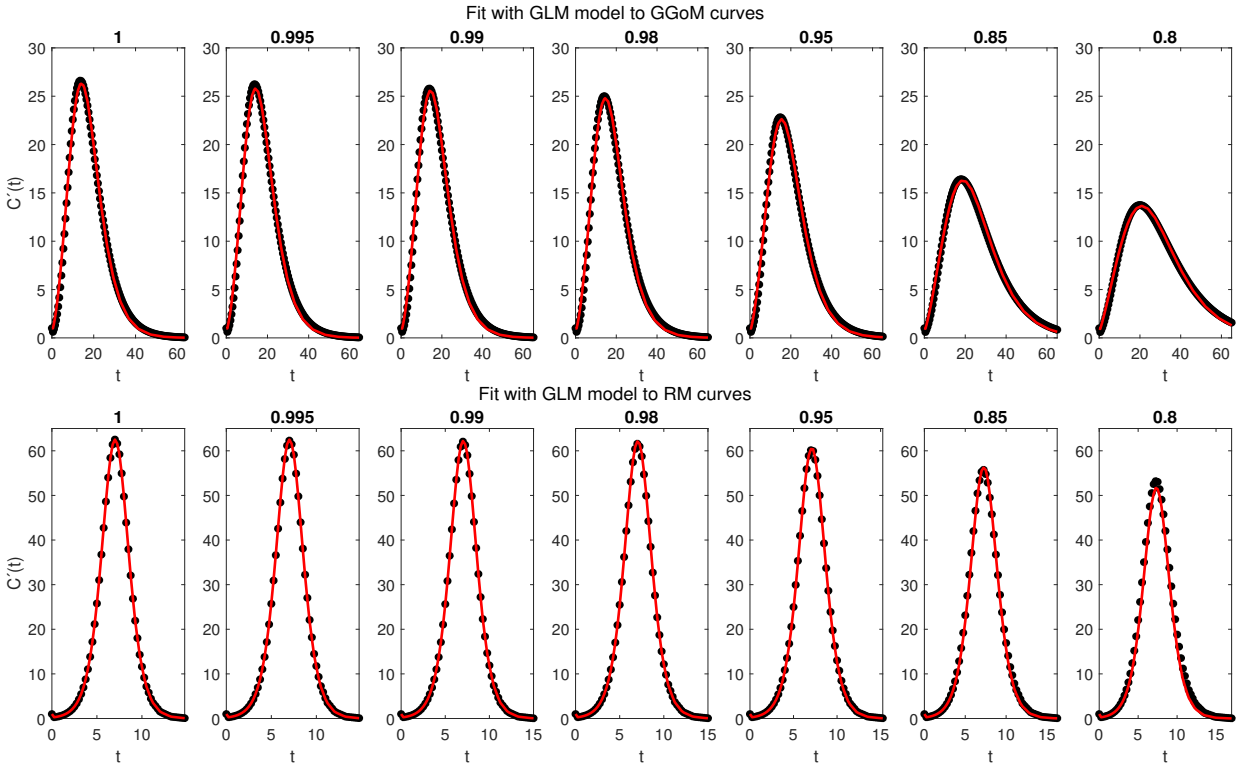

FIGURE 7. Experiment 3: results of fits of the GLM (model B) to the curves of data generated by the GGoM (top row) and the RM (bottom row), for the indicated values of p.

dynamics presented for the GLM data curves. Now with the RMSE calculated, we have effectively the smallest errors for the fit to GLM data, where in Table 5 we see that the RMSE increases faster with GGoM data than with GLM data. Besides, the RMSEs for GLM curves are less than 0.5, evidencing relative closeness between the logistic models. Concerning the the parameter estimation (Table 7), we have a good approximation between the parameters for GLM when $p = 1$, where the estimated parameter p varies more than the growth rate r to capture the decrease of the maximum value, evidencing a good contribution of this parameter. On the other hand the variation of the parameter r is smaller than that of p and K when the RM is used to fit the GGoM curves.

3.5. **Experiment 3: distances from the generalized logistic model (GLM) to other models.** In Figure 7, we can see a performance closer to both dynamics with GLM, where this model captures fairly well the maximum value and the length time. Observing the RMSEs (5), we can see that these are smalller than 1.6, as expected when we consider the fits shown in Figure 7. Now, analyzing Table 5 we observe that the errors increase faster for RM (when p decreases) than with GGoM, where the errors decrease slowly when p decreases. This behavior may be due to the dynamics of the GLM, where if the maximum value decreases, the time length increases, but for the RM data curves, the time length and maximum value are closer to each other. About parameter estimation (see Table 8), we have that for the parameter set with the RM curves the values are closer to parameters to GLM model with $p = 1$, i.e, $\Theta = (0.999, 1, 1000)$. This, because, the RM curves vary little of the RM initial curve with $p = 1$. The previous result contrasts with the fit

Parameter Estimation for GLM						
CURVES	with GGoM curves			with RM curves		
with p	r	p	K	r	p	K
1	1.5402	0.6744	998.0430	0.9994	0.9999	1000.1965
0.995	1.5293	0.6734	986.8504	1.0000	0.9999	999.3734
0.99	1.5054	0.6743	989.5241	1.0000	0.9991	1000.4114
0.98	1.5221	0.6670	992.3809	1.0000	0.9984	1003.5106
0.95	1.5278	0.6508	992.7939	1.0000	0.9961	992.1099
0.85	1.5204	0.5962	994.5254	1.0000	0.9876	971.7100
0.8	1.5112	0.5678	989.0751	0.9888	0.9850	915.3278

TABLE 8. Experiment 3: parameter estimation for GLM with GGoM and RM data curves .

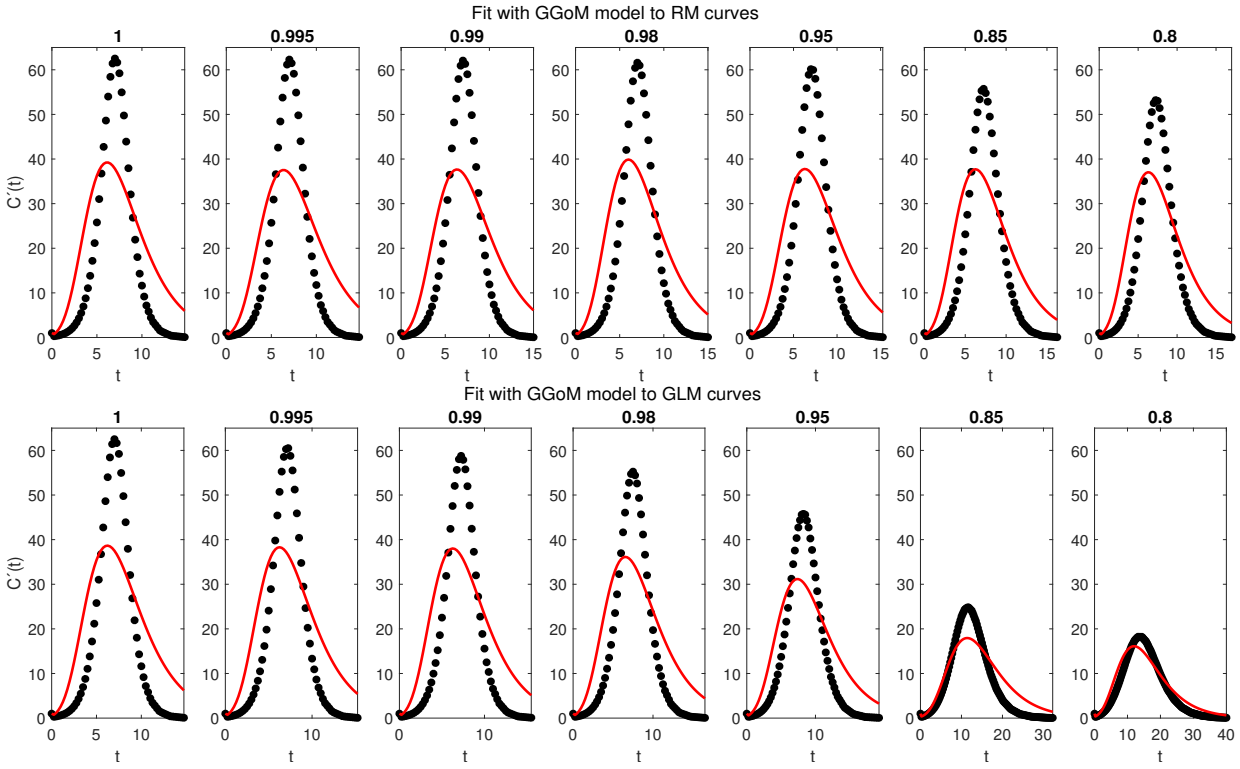

FIGURE 8. Experiment 4: results of fits of the GGoM (model B) to the curves of data generated by the RM (top row) and the GLM (bottom row), for the indicated values of p.

for GGoM curves, because when the parameter p varies for GGoM curves, the maximum value decreases and the time length increases, where with the GGoM the length time is the same when the parameter p decreases. For this reason the parameter estimation for the GGoM curves varies the parameter p more than others.

Parameter estimation for GGoM						
CURVES	with GLM curves			with RM curves		
with p	r	b	p	r	b	p
1	2.3207	0.3237	1.0000	2.3516	0.3279	1.0000
0.995	2.3068	0.3220	1.0000	2.2635	0.3159	1.0000
0.99	2.2932	0.3201	1.0000	2.2761	0.3178	1.0000
0.98	2.1953	0.3068	1.0000	2.4303	0.3326	0.9948
0.95	1.9338	0.2712	1.0000	2.2822	0.3187	1.0000
0.85	1.2596	0.1678	0.9823	2.2986	0.3214	1.0000
0.8	1.2670	0.1500	0.9496	2.2716	0.3180	1.0000

TABLE 9. Experiment 4: parameter estimation for GGoM with GLM and RM data curves.

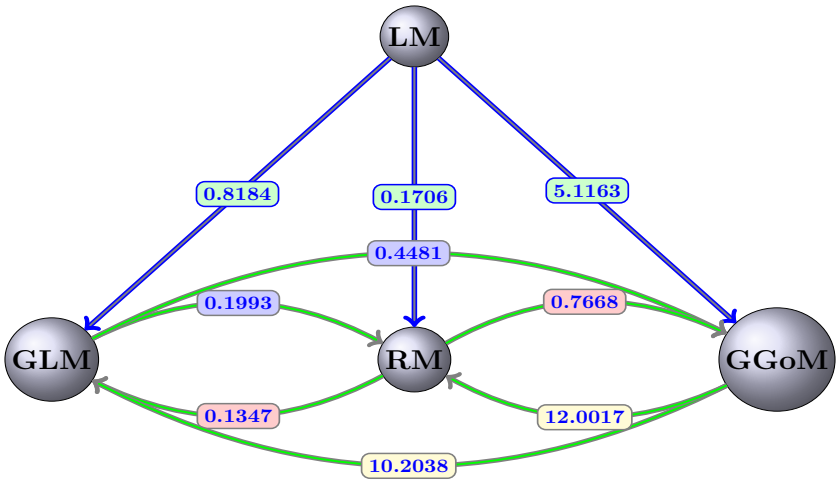

FIGURE 9. Comparative graph for each distance and model.

3.6. **Experiment 4: distances from the generalized Gompertz model (GGoM) to other models.** For this experiment, we consider the GGoM model as model B, and the models A are RM and GLM, with the parameters summarized in Table 2. In Figure 8 we can see the fits for RM and GLM data curves. This figure indicates that the GGoM does not capture the dynamics of the logistic models, where the maximum values are very large for the period of time defined in these data curves. The RMSEs in Table 5 are very large if compared with the previous experiments. The errors decrease when the parameter p is decreased, but this situation is due to approximation between the maximum values of the data curves and the maximum value that the GGoM can reach with the given period of time.

Finally, the parameter estimation obtained for each fit is summarized in Table 9, where we observe that the parameter p is almost fixed. Being for the RM curves the other parameters almost equally fixed, this is due to the slow decrease for the maximum value. This contrasts with the result for the GLM, where the maximum value decreases faster than for the RM. For this reason

	Influenza		Ebola		COVID-19	
Model	Interpolation	No interpolation	Interpolation	No interpolation	Interpolation	No interpolation
LM	28.4864	55.5662	44.5472	90.0674	59.6479	108.9944
GLM	26.2694	49.7601	24.4430	47.8958	21.2940	45.4623
GGoM	52.7972	113.9227	51.8345	94.6347	174.9620	356.6672
RM	29.1628	55.8399	26.2160	53.3493	54.9620	109.9705

TABLE 10. Application to real data: RSME for different time refinements.

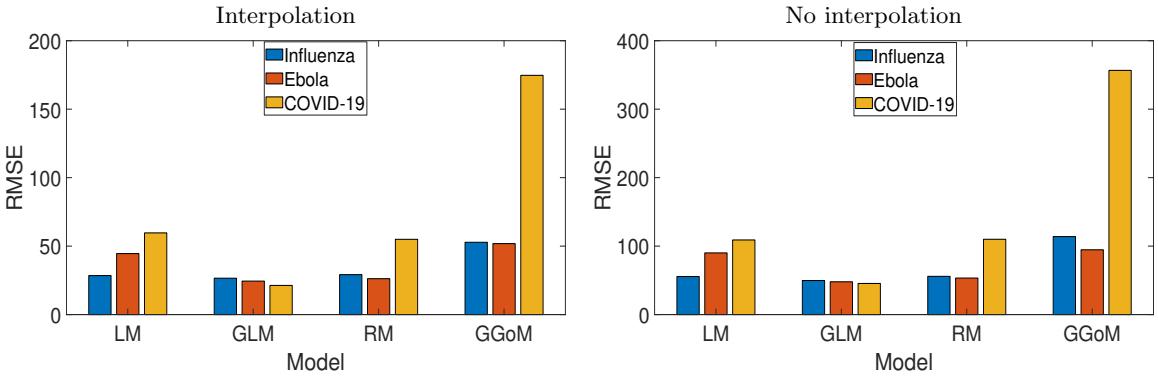

FIGURE 10. Application to real data: bar charts for the RMSE for each real data and refinement time.

	Influenza	Ebola	COVID-19
Model		Interpolation	
LM	$(0.5561, 2467.9)$	$(0.3141, 8988.2)$	$(0.3413, 9074.6586)$
GLM	$(0.5964, 1, 2228.8)$	$(0.7481, 0.8546, 10989)$	$(3.6232, 0.6869, 12963.9057)$
GGoM	$(1.244, 0.1809, 1)$	$(1.0000, 0.0897, 0.9487)$	$(5.7818, 0.0989, 0.6709)$
RM	$(0.5603, 1, 2655.7)$	$(0.4189, 0.4273, 11057)$	$(0.4188, 0.6302, 9196.4353)$
		No interpolation	
LM	$(0.5565, 2475.9)$	$(0.3127, 8327.7)$	$(0.3426, 9844.7509)$
GLM	$(0.6003, 1, 2363.1)$	$(0.7640, 0.8515, 11212)$	$(2.7782, 0.7213, 12316.4258)$
GGoM	$(1.2434, 0.1800, 1)$	$(0.8134, 0.0968, 1.0000)$	$(5.0086, 0.1020, 0.6931)$
RM	$(0.55451, 2392.5)$	$(0.4326, 0.4000, 11698)$	$(0.4133, 0.6472, 9145.3252)$

TABLE 11. Application to real data: parameter estimation for fit with real data

the parameters r and b are varying. Summarizing, we have in Figure 9 the distances presented among the models studied, where each arrow indicates the direction of the distance from model B to model A.

4. Examples: application to real data

In order to see the best performance evidenced by the GLM model, when capturing the other dynamics studied in the experiments performed, we present three examples with real data. In this

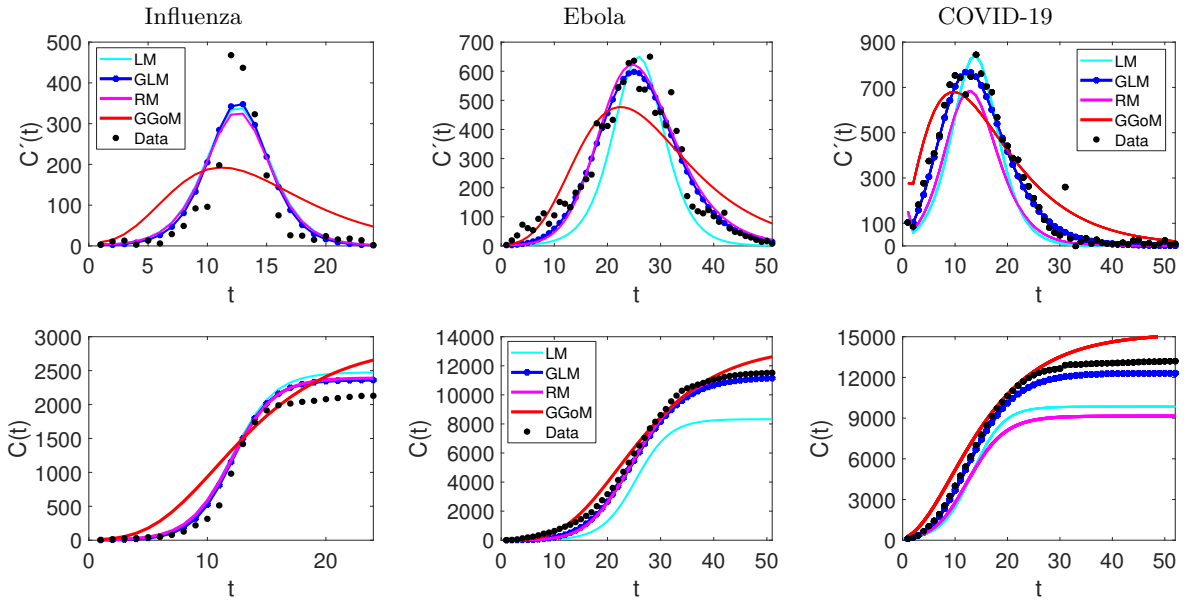

FIGURE 11. Application to raw data: fits to influenza, Ebola and COVID-19 data.

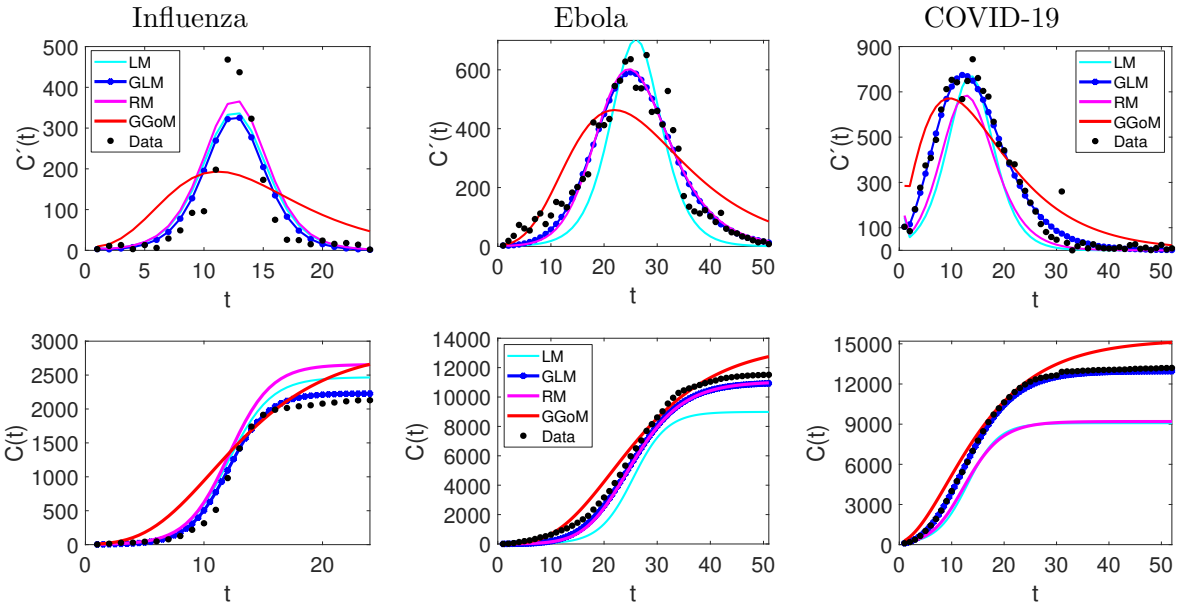

FIGURE 12. Application to interpolated data: fits to influenza, Ebola and COVID-19 data.

case, we consider the data of weekly cases of influenza in Chile (24 data points in total) produced between autumn and winter of 2009 [38], Ebola (51 data points in total) in Sierra Leona dating from 2014 [39] and recent outbreak of COVID-19 [40] presented in various provinces of China (excluding Hubei province) (52 data points in total). Since we consider real data, for the application of the procedure of Section 3 we replace model A by real data but keep employing the same methodology

of Section 3 with model B, where we also create a refinement of the real data by interpolation from the cumulative curve C, achieving for these examples twice the original number of points. From the RMSEs calculated and registered in Table 10 and the bar chart of Figure 10 we observe that the RMSEs for the non-interpolated data are close to the double from the RMSEs for the interpolated data, where effectively GLM meets be the best model with the smaller RMSE to the three examples.

From the figures of the fits, with and without interpolation (see Figures 11 and 12) for three examples, we can observe that the refinement from real data does not have a great impact on the performance of the GGoM (red), but this model for early growth in Ebola case produces a better fit than other models. For the fits made with the LM, we can observe that for the case of influenza the refinement leaves the fit similar to a fit without interpolation where for this case, the LM is better than the RM. A different situation occurs for the Ebola and COVID-19 cases where for Ebola the maximum value for the incidence curve increases and the cumulative curve increases close to real cumulative curve, though this is not better than the fits by the GLM and the RM. For COVID-19 the LM decreases the maximum value for the incidence curve and the cumulative curve decreases close to the cumulative curve of the RM, although this is not better than the fits by the GLM and RM. Now if we observe the fits with the RM and the GLM, we see that their fits though very similar for Ebola data, the GLM fits are better where the RMSE is smaller. On the other hand, with influenza data, we can see that for RM and GLM models, the fits to real data, the curve with GLM is above the RM curve, staying in the middle the LM curve, and the situation changes when the data are interpolated, where the RM curve turns out to be above the GLM and LM curves, but the GLM produces the best fit with the smallest RMSE. In the case of the COVID-19, the fits with the GLM with and without interpolated data are very close. A different situation occurs with the RM where the fits to the interpolated and non-interpolated data are below the data and therefore with RMSEs bigger than the RMSEs for GLM. Furthermore, Table 11 indicates that for the parameter estimation the values are very close between the real data and interpolated data, where for the LM this shows smaller variations and the GGoM model shows more variations with Ebola data.

Finally, an important observation in these examples is that besides being closer to the other dynamics, the GLM also captures better real data due the advantageous contribution of the growth scaling parameter p. This fact is also demonstrated in [16]. However, this same parameter p can have another nature in the RM, where there are studies with $p > 1$, for example, the papers [41,42], where we recall that in [16] it was stated that the parameter p as growth scaling parameter does not achieve to capture the sub-exponential growth which very important to studies of early epidemic growth. Then if we consider the case $p > 1$ the RM, we can see that this model captures the dynamics of influenza data better than the GLM, as is evidenced in Figure 13 and Table 12,.

With respect to the parameter p in [42] we comment that this parameter has another nature in the Richards model, different from a scaling parameter, where in this position could allow the shape of upper part of the cumulative curve to be independent of the shape of the lower part, i.e., measures the extent of deviation from the S-shaped dynamics of the classical logistic growth model. Besides, as the parameter p tends to zero, the RM curve tends towards the Gompertz growth curve in the sense $\mathrm{d}C/\mathrm{d}t = rC(t)\ln(K/C(t))$. There are other studies on different forms to generalize growth models, as [41] which shows for case of logistic growth, different to our idea of generalized growth model with $rC(t)^p$, being p a scaling parameter. Therefore future work will study the distances between other generalized growth models.

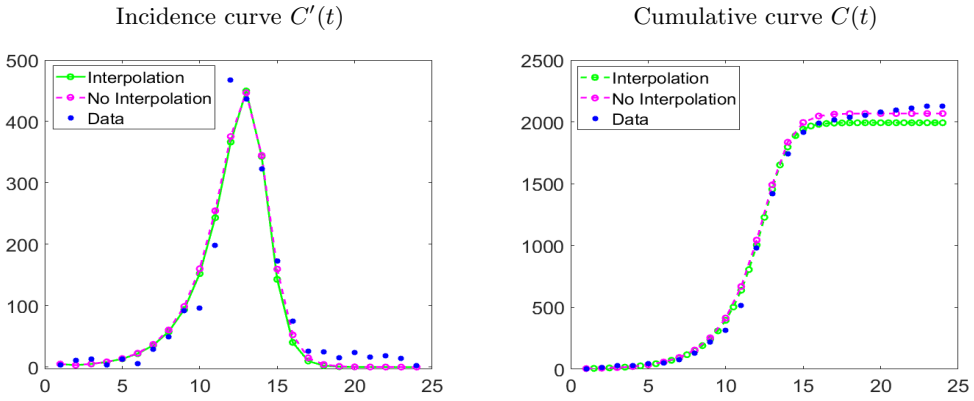

FIGURE 13. Application to real data: fits with Richards Model ($p > 1$) for influenza data.

Results	Influenza	Ebola	COVID-19
	Interpolation		
RMSE	17.2332	26.2223	46, 9405
Parameter Estimation	(0.4883, 3, 1993.2)	(0.4173, 0.4308, 11036)	(0.4551, 0.5408, 9895.1873)
	No interpolation		
RMSE	28.7735	51.6678	100, 3531
Parameter Estimation	(0.49, 2.6641, 2068.1)	(0.4228, 0.4191, 11182)	(0.4350, 0.5877, 9556.1028)

TABLE 12. Application to real data: results for different time refinements and real data for RM model with $p > 1$.

5. Conclusions

Overall methodology applied to these five models for three different types of growth curves, we can say that the GLM model is closer to the other models and the GGoM model is the most distant. Besides, the parameter p contributes significantly for the logistic models GLM and RM since the approximation achieved with the LM is substantially improved with this extra parameter. In contrast with GGoM result, where the parameter estimation show that $p \approx 1$ in most fits, i.e., GGoM is being reduced to GoM with parameters $\Theta = (r, b)$ with $p = 1$.

Acknowledgments

RB is supported by Fondecyt project 1170473; CONICYT/PIA/AFB170001; and CRHIAM, project ANID/FONDAP/15130015. GC acknowledges financial support from grants NSF-IIS RAPID award #1518939, NSF grant 1318788 III: Small: Data Management for Real-Time Data Driven Epidemic simulation, and Conicyt (Chile), project MEC80170119. LYLD is supported by CONICYT scholarship CONICYT-PCHA/Doctorado Nacional/2019-21190640.

References

[1] G. Chowell, Fitting dynamic models to epidemic outbreaks with quantified uncertainty: A primer for parameter uncertainty, identifiability, and forecast, Infect. Disease Model. 2 (2017) 379–398.

[2] P.-F. Verhulst, Notice sur la loi que la population suit dans son accroissement, Corresp. Math. Phys. 10 (1838) 113–121.

[3] B. Gompertz, On the nature of the function expressive of the law of human mortality, and on a new mode of determining the value of life contingencies, Phil. Trans. R. Soc. Lond. 115 (1825) 513–583.

[4] F.J. Richards, A flexible growth function for empirical use, J. Exp. Bot. 10 (1959) 290–301.

[5] X.S. Wang, J. Wu, Y. Yang, Richards model revisited: Validation by and application to infection dynamics, J. Theor. Biol. 313 (2012) 12–19.

[6] J.D. Murray, Mathematical Biology: I. An Introduction, Springer-Verlag, New York, 2002.

[7] D.S. Jones, B.D. Sleeman, Differential Equations and Mathematical Biology, Chapman & Hall/CRC, Boca Raton, FL, 2003.

[8] N.F. Britton, Essential Mathematical Biology, Springer-Verlag, London, 2003.

[9] F. Brauer, C. Castillo-Chavez, Mathematical Models in Population Biology and Epidemiology, Second Ed., Springer, New York, 2012.

[10] O. Diekmann, J. Heesterbeek, T. Britton, Mathematical Tools for Understanding Infectious Disease Dynamics, Princeton Series in Theoretical and Computational Biology, Princeton University Press, 2012.

[11] L.A. Segel, L. Edelstein-Keshet, A Primer on Mathematical Models in Biology, SIAM, Philadelphia, PA, 2013.

[12] M.E. Turner Jr., E.L. Bradley, Jr., K.A. Kirk, K.M. Pruitt, A theory of growth, Math. Biosci. 29 (1976) 367–373.

[13] F. Brauer, C. Kribs, Dynamical Systems for Biological Modeling: An Introduction, CRC Press, Boca Raton, FL, USA, 2016.

[14] R.M. Anderson, R.M. May, Infectious Diseases of Humans, Dynamics and Control, Oxford University Press, 1991.

[15] P. Yan, G. Chowell, Quantitative Methods for Investigating Infectious Disease Outbreaks, Springer Nature, Cham, Switzerland, 2019.

[16] R. Bürger, G. Chowell, L.Y. Lara-Díaz, Comparative analysis of phenomenological growth models applied to epidemic outbreaks, Math. Biosci. Eng. 16 (2019) 4250–4273.

[17] G. Chowell, H. Nishiura, L.M.A. Bettencourt, Comparative estimation of the reproduction number for pandemic influenza from daily case notification data, J. R. Soc. Interface 4 (2007) 155–166.

[18] A.R. Arenas, N.B. Thackar, E.C. Haskell, The logistic growth model as an approximating model for viral load measurements of influenza A virus, Math. Comput. Simulation 133 (2017) 206–222, ISSN 0378-4754 (doi.org/10.1016/j.matcom.2016.10.002).

[19] G. Chowell, C. Viboud, J.M. Hyman, L. Simonsen, The Western Africa Ebola virus disease epidemic exhibits both global exponential and local polynomial growth rates, PLOS Currents Outbreaks 7 (2015) (21 January).

[20] G. Chowell, C. Viboud, L. Simonsen, S. Merler, A. Vespignani, Perspectives on model forecasts of the 2014–2015 Ebola epidemic in West Africa: lessons and the way forward, BMC Medicine 15 (2017) paper 42 (8pp).

[21] B. Pell, Y. Kuang, C. Viboud, G. Chowell, Using phenomenological models for forecasting the 2015 Ebola challenge, Epidemics 22 (2018) 62–70.

[22] G. Chowell, D. Hincapie-Palacio, J. Ospina, B. Pell, A. Tariq, S. Dahal, S. Moghadas, A. Smirnova, L. Simonsen, C. Viboud, Using phenomenological models to characterize transmissibility and forecast patterns and final burden of Zika epidemics, PLoS Currents Outbreaks, Edition 1, 31 May 2016 (doi: 10.1371/currents.outbreaks.f14b2217c902f453d9320a43a35b9583).

[23] M. Brown, C. Cain,J. Whitfield, E. Ding, S.Y. Del Valle, C.A. Manore, Modeling Zika virus spread in Colombia using Google search queries and logistic power models. Preprint bioRxiv 365155 (2018); doi: https://doi.org/10.1101/365155

[24] K. Mitsumoto, K. Kagaya, G. Chowell, Early epidemiological assessment of the transmission potential and virulence of 2019 Novel Coronavirus in Wuhan City: China, 2019–2020, Preprint (2020), medRxiv, doi: https://doi.org/10.1101/2020.02.12.20022434.

[25] K. Roosa, Y. Lee, R. Luo, A. Kirpich, R. Rothenberg, J.M. Hyman, P. Yan, G. Chowell, Real-time forecasts of the COVID-19 epidemic in China from February 5th to February 24th, 2020, Infect. Disease Model. 5 (2020) 256–263.

[26] D. Faranda, I. Pérez Castillo, O. Hulme, A. Jezequel, J.S.W. Lamb, Y. Sato, E.L. Thompson, Asymptomatic estimates of SARS-CoV-2 infection counts and their sensitivity to stochastic perturbation, Chaos 30, 051107 (2020); doi: 10.1063/5.0008834.

[27] M. Catala, S. Alonso, E. Alvarez-Lacalle, D. Lopez, P.J. Cardona, C. Prats, Empiric model for short-time prediction of COVID-19 spreading, Preprint (2020), medRxiv, doi: https://doi.org/10.1101/2020.05.13.20101329
[28] G. Chowell, Fitting dynamic models to epidemic outbreaks with quantified uncertainty: A primer for parameter uncertainty, identifiability, and forecast, Infect. Disease Model. 2 (2017) 379–398.
[29] E. Vynnycky, R.G. White, An Introduction to Infectious Disease Modelling, Oxford University Press, 2010.
[30] G. Chowell, C. Viboud, L. Simonsen, S.M. Moghadas, Characterizing the reproduction number for epidemics with sub-exponential growth dynamics, J. Roy. Soc. Interface 13 (2016) paper 20160659 (12pp).
[31] R.V.V. Vidal, Applied Simulated Annealing. Lecture Notes in Economics and Mathematical System, Springer-Verlag, Berlin, Germany, 1993.
[32] P. Román-Román, D. Romero, M.A. Rubio, F. Torres-Ruiz, Estimating the parameters of a Gompertz-type diffusion process by means of Simulated Annealing, Appl. Math. Comput. 218 (2012) 5131–5131.
[33] M. Kühleitner, N. Brunner, W.-G. Nowak, K. Renner-Martin, K. Scheicher, Best-fitting growth model curves of the Bertalanffy-Pütter type, Poultry Science 98 (2019) 3587–3592.
[34] C. Viboud, L. Simonsen, G. Chowell, A generalized-growth model to characterize the early ascending phase of infectious disease outbreaks, Epidemics 15 (2016) 27–37.
[35] G. Chowell, C. Viboud, Is it growing exponentially fast?—Impact of assuming exponential growth for characterizing and forecasting epidemics with initial near-exponential growth dynamics, Infect. Disease Model. 1 (2016) 71–78.
[36] G. Chowell, L. Sattenspiel, S. Bansal, C. Viboud, Mathematical models to characterize early epidemic growth: A review, Physics of Life Rev. 18 (2016) 66–97.
[37] S. Ohnishi, T. Yamakawa, T. Akamine, On the analytical solution of the Pütter-Bertalanffy growth equation, J. Theor. Biol. 343 (2014) 174–177.
[38] Ministerio de Salud Chile, Influenza Pandemia (H1N1) 2009. Circular de Vigilancia epidemiología de influenza. Available from: http://epi.minsalud.cl/epi/html/normas/circul/CircularInfluenzaESTACIONALyPANDEMICA.pdf.
[39] 2015 Ebola response roadmap—Situation report—14 October 2015. See http://apps.who.int/ebola/current-situation/ebola-situation-report-14-october-2015 (accessed 17 October 2015).
[40] Chinese National Health Committee. Reported cases of 2019-nCoV. Retrieved from https://ncov.dxy.cn/ncovh5/view/pneumonia?from=groupmessage&isappinstalled=0.
[41] A. Tsoularis, J. Wallace, Analysis of logistic growth models, Math. Biosci. 179 (2002) 21–55. See https://doi.org/10.1016/S0025-5564(02)00096-2.
[42] C. Birch, A new generalized logistic sigmoid growth equation compared with the Richards growth equation, Annals of Botany 83 (1999) 713–723, doi: https://doi.org/10.1006/anbo.1999.0877.